

Synthesis and Characterization of Heterobimetallic (Pd/B) Nindigo Complexes and Comparisons to Their Homobimetallic (Pd₂, B₂) Analogues

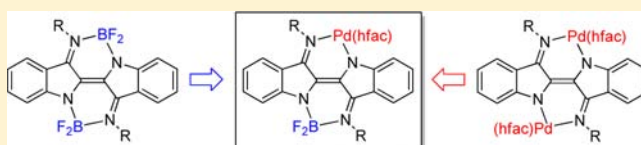
Graeme Nawn,[†] Robert McDonald,[‡] and Robin G. Hicks^{*,†}

[†]Department of Chemistry, University of Victoria, P.O. Box 3065, STN CSC, Victoria, British Columbia, V8W 3V6, Canada

[‡]Chemistry Department, University of Alberta, 11227 Saskatchewan, Drive NW, Edmonton, Alberta, T6G 2G2, Canada

Supporting Information

ABSTRACT: Reactions of Nindigo-BF₂ complexes with Pd(hfac)₂ produced mixed complexes with Nindigo binding to both a BF₂ and a Pd(hfac) unit. These complexes are the first in which the Nindigo ligand binds two different substrates, and provide a conceptual link between previously reported bis(BF₂) and bis(Pd(hfac)) complexes. The new Pd/B complexes have intense near IR absorption near 820 nm, and they undergo multiple reversible oxidations and reductions as probed by cyclic voltammetry experiments. The spectral, redox, and structural properties of these complexes are compared against those of the corresponding B₂ and Pd₂ complexes with the aid of time-dependent density functional calculations. In all cases the low-energy electronic transitions are ligand-centered $\pi-\pi^*$ transitions, but the highest occupied molecular orbital (HOMO) and lowest unoccupied molecular orbital (LUMO) energies—and hence the absorption wavelength as well as the oxidation and reduction potentials—are significantly modulated by the moieties bound to the Nindigo ligand.

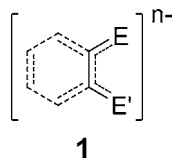


INTRODUCTION

Metal complexes containing redox-active ligands (RALs) have long fascinated inorganic chemists because of the special challenges associated in elucidating their electronic structure (i.e., “where are the valence electrons?”).¹ Indeed, fundamental studies of this sort have constituted a branch of physical inorganic chemistry for over 50 years. In more recent times, the possibility of harnessing ligand redox activity in stoichiometric and catalytic reaction chemistry has led to a huge increase in interest in RAL complexes.² That two recent issues of leading inorganic chemistry journals have devoted special issues to this subject serve as testimony to the high level of activity in contemporary RAL complex chemistry.³

By far the most common RALs are based on the “1,4-heterodiene” skeleton **1** (Scheme 1) where E/E' = O/O

Scheme 1

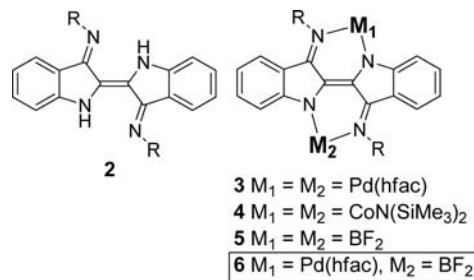


(dioxolenes), S/S (dithiolenes), N/N (α -diimines), as well as mixed-donor analogues (e.g., E/E' = O/N), and tri- and tetradentate analogues. Not surprisingly these ligands have attracted the most attention in the context of reactivity and catalysis.⁴ Other recent examples of novel reactivity and catalysis using RALs based on, for example, 2,6-diiminopyr-

ridines,⁵ carbene radicals,⁶ aminyl radicals,⁷ and π -conjugated organometallics⁸ highlight the motivations and possible benefits of designing and discovering new kinds of RALs.

We recently introduced Nindigo **2** as a new type of RAL which can be made in a straightforward manner directly from the famous pigment indigo.⁹ The Nindigo ligand system is distinguished by (i) its ability to coordinate two metals via two β -diketiminato-type binding sites, (ii) the intense visible/near-infrared absorption of the ligand and its complexes, and (iii) an exceptional degree of ligand-centered redox-activity—the ligand can adopt charge states ranging from 0 to -4 . Transition metal complexes of Nindigo are limited so far to bis-palladium¹⁰ and bis-cobalt¹¹ complexes **3** and **4** respectively; bis-boron¹² species **5** have also been reported, expanding the repertoire of Nindigo complexes into the p-block (Scheme 2).

Scheme 2



Received: April 12, 2013

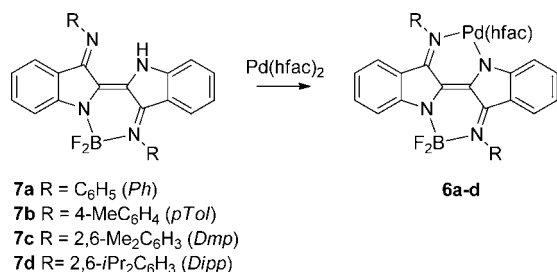
Published: September 20, 2013

In all of these examples the rich electronic absorption spectra and redox properties have been ascribed to the ligand, but clearly the metal fragment bound to the ligand plays an important role in determining the specific (ligand-centered) physicochemical features. Herein we present the synthesis of complexes **6**, the first mixed-metal Nindigo coordination complexes. Because these molecules contain one boron and one palladium moiety, they provide a conceptual bridge between the previously reported complexes **3** and **5** and offer the opportunity to examine how the electronic structure (as manifested by the redox and spectroscopic properties) of Nindigo complexes evolves as a function of what it is coordinated to.

RESULTS AND DISCUSSION

Synthesis and Characterization of Nindigo PdB Complexes. We previously reported that reactions of Nindigo with BF_3 can be optimized either to produce bis- BF_2 complexes **5** or mono- BF_2 species **7**, the latter of which contains a remaining open coordination site.¹² Reaction of derivatives of **7** with $\text{Pd}(\text{hfac})_2$ led to Pd/B complexes **6** in good (>70%) yields (Scheme 3). Unlike the bis- BF_2 complexes **5**, which slowly

Scheme 3



decompose via the elimination of one BF_2 unit to give **7**,¹² the heterobimetallic complexes **6** are stable in solution as well as the solid state. The NMR spectroscopic properties of **6** bear strong resemblances to the homometallic species **3** and **5**: The ^{11}B NMR spectra consist of a triplet ($J_{\text{FB}} \sim 29$ Hz) at ~ 1.5 ppm, while the ^{19}F spectra contain resonances for the two inequivalent CF_3 groups (~ -74 and -75 ppm) and a quartet at about -130 ppm ($J \sim 29$ Hz) due to the BF_2 fluorine atoms.

X-ray Structures. X-ray structures were obtained for all derivatives of **6** except the *p*-tolyl compound **6b**. The three structures have qualitatively similar features; the structure of **6a** is shown in Figure 1 as a representative example. The coordination geometries at boron and palladium are approximately tetrahedral and square planar, respectively. The Nindigo ligand “core” (i.e., excluding the imine and its substituent) of **6d** is planar; there is a slight bowing of the core of the ligands in **6a** and **6c** creating concave and convex surfaces on the ligand (see Supporting Information). This bowing can be quantified by a dihedral angle defined by the planes of the two benzannulated benzene rings of the ligand; for **6a** this angle is 16.1° while for **6c** the values (for each of the two molecules in the asymmetric unit) are 8.0° and 6.9° (for **6d** the angle is 0.8°). Both of the N-aryl substituents of each complex are nearly orthogonal to the plane of the ligand core. In each of the three structures the coordinated atoms lie in or close to the plane defined by its NCCCN chelate (the maximum deviation from chelate planarity for the Pd ions is 0.47 Å for **6a** and for B is 0.31 for **6c**). The ligand-based bond

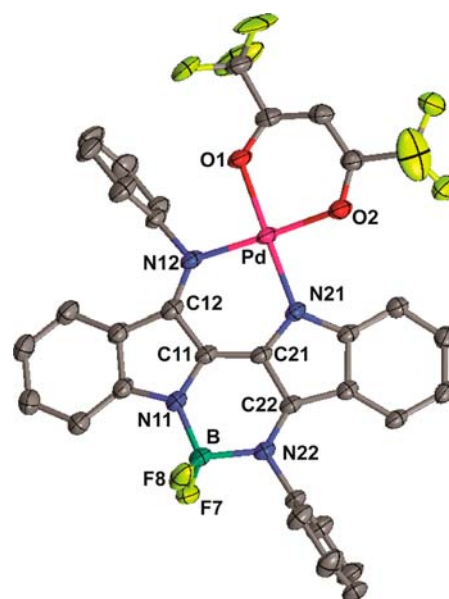
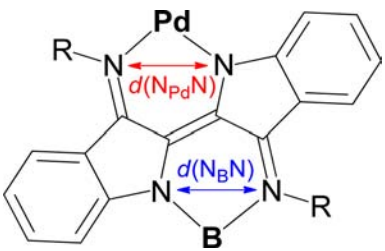


Figure 1. X-ray structure of **6a**. Thermal ellipsoids set at 50%; hydrogen atoms omitted for clarity. Selected bond lengths (Å): Pd–O1 2.0227(18), Pd–O2 2.0129(19), Pd–N21 1.9969(19), Pd–N12 2.019(2), B–N22 1.588(4), B–N11 1.538(3), B–F7 1.397(4), B–F8 1.371(4), C11–C21 1.365(3), C11–C12 1.449(3), C21–C22 1.449(3), N11–C11 1.358(3), N12–C12 1.323(3), N21–C21 1.366(3), N22–C22 1.314(3). Selected bond angles (deg): O1–Pd–O2 90.39(8), N11–Pd–N22 92.57(8), F7–B–F8 109.5(2), N11–B–N21 107.6(2).

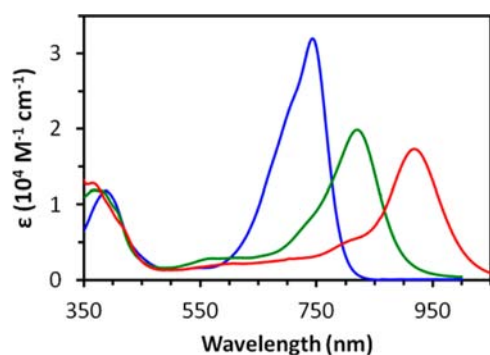
metrics are comparable to those seen in the structures of derivatives of **3** and **7** (as well as those for the ligands **2**) and are indicative of a high degree of delocalization within the central portion of the Nindigo ligand core.

There are subtle but important differences between some of the metrics of the structures of **6** and the corresponding structures of both Nindigo-boron complexes **7** and Nindigo-palladium structures **3** (Table 1). Starting with the boron binding site, the mean B–N bond length to the indolide nitrogen is essentially the same in **6** and **7**. However, the BN(imine) bond in **6** is on average slightly longer relative to that in **7**. Similar trends are evident in comparing the Pd–N bonds in **6** to those in the Pd $_2$ complexes **3**. Finally the (nonbonded) distance between the pair of nitrogen atoms binding to B and the pair binding to Pd are quite different in **6** (2.514 and 2.935 Å respectively). These differences are due to the relative sizes of the B and Pd ions and the Nindigo ligand’s ability to accommodate two differently sized elements. No structural data on the B $_2$ complexes **5** is available, and we previously suggested that the low stability associated with these is due to the poor fit for two boron atoms: the mono-B structures show opening up of the noncoordinated site as a consequence of the other one pinching in to bind B.¹² In the Pd/B structures the disparate sizes of the two elements can be accommodated in the Nindigo bis-chelate.

Electronic Spectra. The spectral characteristics of **6a–6d** are nearly identical to one another; each compound has an intense absorption near 820 nm with extinction coefficients of about $20,000 \text{ M}^{-1} \text{ cm}^{-1}$. The λ_{max} values for **6** fall in between those of corresponding derivatives of bis-boron species **5** ($\lambda_{\text{max}} \sim 750$ nm) and bis-palladium species **3** ($\lambda_{\text{max}} \sim 920$ nm) (Figure 2). We previously assigned the origin of the low-energy absorption of **3** as a ligand-based π – π transition,¹⁰ and our

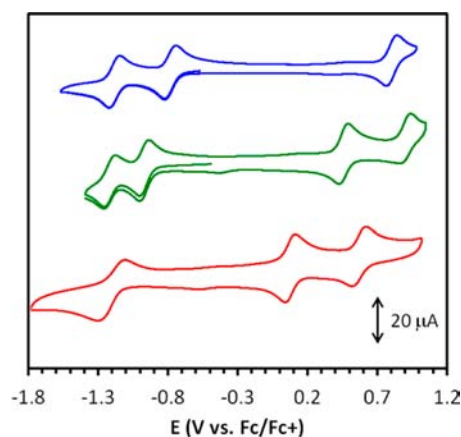
Table 1. Average Selected Distances (Å) in **6** and Related Species


	$d(\text{BN}_{\text{imine}})$	$d(\text{BN}_{\text{indolide}})$	$d(\text{N}_{\text{B}}\text{N})$	$d(\text{PdN}_{\text{imine}})$	$d(\text{PdN}_{\text{indolide}})$	$(\text{N}_{\text{Pd}}\text{N})$
6	1.585 ± 0.005	1.533 ± 0.004	2.514 ± 0.011	2.025 ± 0.007	2.003 ± 0.007	2.935 ± 0.026
7	1.560 ± 0.005	1.530 ± 0.004	2.504 ± 0.004			
3				1.999 ± 0.016	1.985 ± 0.009	2.845 ± 0.019

Figure 2. Electronic spectra of **3b** (red), **5b** (blue), and **6b** (green) in CH_2Cl_2 .

computational studies on derivatives of **5** also indicated that their lowest energy absorption are due to π - π transitions.¹²

Electrochemical Studies. The cyclic voltammogram (CV) of **6a** is presented in Figure 3 as a representative example; the

Figure 3. CVs of **3a** (red), **5a** (green), and **6a** (orange) (CH_2Cl_2 solution, ~ 0.1 mM analyte, 0.1 M Bu_4NBF_4 electrolyte, scan rate 100 $\text{mV}\cdot\text{s}^{-1}$).

CVs of analogous complexes **3a** and **5a** are also presented for comparative purposes. Electrochemical data for derivatives of **6** and related species are compiled in Table 2. Our previous electrochemical studies of bis-palladium complexes **3** revealed two reversible one-electron oxidation processes and a single two-electron reduction.¹⁰ In contrast, the bis-boron Nindigo complexes **5** have a lone observable one-electron oxidation and two sequential one-electron reductions.¹² The electrochemical

Table 2. Electrochemical Data for **6** and Related Compounds^a

cpd.	reduction	oxidation	E_{cell} (V)
3a ⁹	-1.21^b	$+0.08, +0.57$	1.29
5a ¹²	$-1.19, -0.79$	$+0.80$	1.59
6a	$-1.22, -0.97$	$+0.46, +0.91^c$	1.43
6b	$-1.26, -1.02$	$+0.44, +0.94^c$	1.46
6c	$-1.64^{d,e}, -1.05$	$+0.48, +0.93$	1.53
6d	$-1.67^{d,e}, -1.02$	$+0.50, +0.96$	1.52

^aPotentials are given in V. vs. Fc^+/Fc in CH_2Cl_2 . Except where otherwise indicated, numbers correspond to formal oxidation or reduction potentials. ^bTwo-electron process. ^cQuasi-reversible. ^dIrreversible; number corresponds to peak potential. ^eMultielectron process.

properties of the mixed Pd/B Nindigo complexes **6** are best described as intermediate between those of **3** and **5**; derivatives of **6** have one reversible and one partially reversible oxidation; the reductive processes depend on the imine substituent. Compounds **6a** and **6b** possess two reversible one-electron reductions, whereas the bulkier derivatives **6c** and **6d** have a single reversible (one-electron) reduction and a second irreversible process that is multielectron in nature (see Supporting Information). The first oxidation and first reduction potentials of **6a** fall in between the corresponding values for **3a** and **5a**: on progressing from **5a**→**6a**→**3a** there is a smooth decrease in both the first oxidation potentials and the first reduction potentials. Interestingly the *second* reduction potential is nearly invariant across this series, with the consequence that for **3a** the first and second reductions “merge” into a single two-electron (quasi-reversible) process which distinguishes the Pd₂ complexes from all other binuclear Nindigo systems, including the Co₂ complexes for which sequential one-electron reductions are observed.¹¹ Two-electron redox processes can be ascribed as examples of “inverted potential”, that is, where the addition of the second reduction is in fact easier than addition of the first.¹³ There is also a discernible trend in the “ E_{cell} ” ($= E_{\text{ox}}^1 - E_{\text{red}}^1$) values, which decrease in the series **5a**→**6a**→**3a**. The trends in $E_{\text{cell}}^{\text{cell}}$ values corroborate the spectroscopic trends described above (Table 2).

Computational Studies. Although the near-infrared activity and rich electrochemical properties of the bis-complexes of Nindigo (**3**, **4**, **5**, and **6**) are nominally ligand-centered, the identity of the “metal” does play a role in influencing the properties. Preliminary computational studies on the boron-based complexes (**5**, **7**) were reported in a

previous paper;¹² herein we present an expansion of these initials studies to include a broader range of compounds, encompassing the Nindigo ligands (**2**) and its boron and/or palladium complexes (**3**, **5**, **6**, **7**) with the goals of exploring structure/property relationships, particularly with respect to the electronic spectroscopy.

Computational studies of organic dyes have received a great deal of attention and considerable effort has gone into examination of the performance of various available functionals. Our choice of the B3LYP functional for these studies was based in part upon the success of this versatile functional in describing the structure and spectroscopy of indigo-based dyes (see below). However, one of B3LYP's limitations is its inconsistent performance in some delocalized systems (e.g., cyanines, charge transfer systems, long chain polyenes). The CAM-B3LYP functional (CAM = Coulomb-Attenuated Method) is an alternative which can provide superior performance in highly delocalized systems; CAM uses a percentage of Hartree–Fock exchange which is distance-dependent, this functional can provide better correlation with experiment than “regular” B3LYP in large delocalized systems.¹⁴ Calculations performed on the series of compounds lead to similarly accurate ground state geometries as for B3LYP. However, CAM-B3LYP performs significantly poorer in terms of correlation with experiment in terms of prediction of the low energy electronic transitions; Table 3 presents the calculated wavelength of the

Table 3. Summary of Computational and Experimental Spectral Data

cpd.	experiment	B3LYP		CAM-B3LYP	
	λ_{\max} /nm	λ_{\max} /nm	$ \Delta ^a/\text{cm}^{-1}$	λ_{\max} /nm	$ \Delta ^a/\text{cm}^{-1}$
indigo	600	589	311	513	2,862
2a	597	624	1451	507	2,972
2c	586	575	326	506	2,679
7a	649	639	241	539	3,145
7c	646	602	1131	523	3,640
5a	744	716	525	637	2,258
5c	746	689	1109	613	2,909
6a	822	807	227	711	1,900
6c	819	792	417	679	2,518
3a	920	900	241	753	2,410
3c		887		743	

^aDifference between calculated and experimental electronic transition energies.

lowest-energy electronic transition for several species along with the corresponding experimental values where available. The CAM-B3LYP functional has been successfully applied to spectroscopic properties of organic dyes through statistical analyses on a large number of closely related structures, which in turns permit empirical corrections to be made.^{14,15} This sort of analysis requires a significantly larger collection of ligands and complexes than is currently available. The B3LYP functional does a significantly better job of predicting lowest energy transitions (and indeed the entire visible spectra of these dyes, see Supporting Information), so the structure/property relationships are developed using the computational results with this functional.

Because of the close relationship of Nindigo to the famous pigment indigo, we opted to begin our computational analysis on the latter molecule. There have been several recent computational studies on indigo employing time-dependent

density functional theory;^{14,16,17} using the B3LYP functional, reasonable size basis sets for both the structure optimization and spectral calculations, and the inclusion of solvent effects through the polarized continuum model, it is possible to accurately predict indigo's low energy electronic transition. Our computational approach (geometry optimization: B3LYP/6-31G* for all elements except for Pd, for which LANL2DZ was employed; time-dependent DFT at the triple- ζ level, with PCM solvation model using CH₂Cl₂) draw collectively from these previous efforts, and perform well in reproducing both indigo's structural metrics (see Supporting Information) and the lowest energy absorption (Table 3); the calculated λ_{\max} of 589 nm is within 11 nm of the experimental value in CH₂Cl₂. As expected, and in agreement with prior studies, the lowest energy transition is predicted to be predominantly on highest occupied molecular orbital (HOMO) to lowest unoccupied molecular orbital (LUMO) based character. These orbitals (Figure 4) are delocalized π orbitals mainly concentrated within

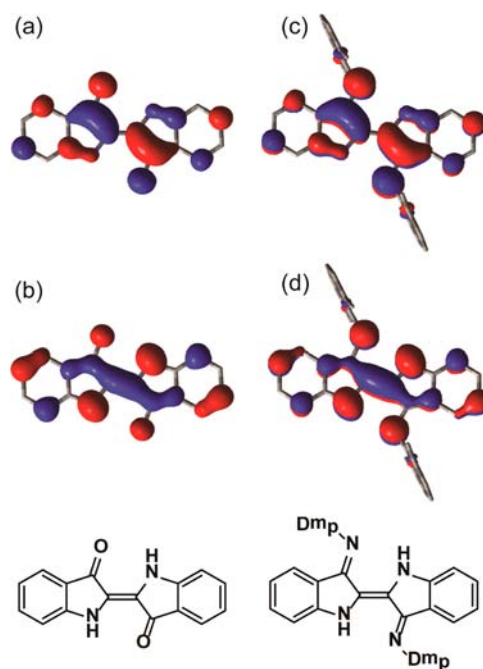


Figure 4. (a) LUMO and (b) HOMO of indigo; (c) LUMO and (d) HOMO of **2c**.

the central C=C bond and adjacent two nitrogens and two carbonyl group. This so-called “H-chromophore” has long been recognized as the principal contributor to the relatively low-energy absorption profile for indigo.¹⁸

We have performed calculations on two derivatives of Nindigo **2** (and the subsequent coordination complexes), namely R = phenyl (Ph; **2a**) and 2,6-dimethylphenyl (Dmp; **2c**). We start with **2c** and compare it to indigo before discussing **2a**. The calculated structure is in good agreement with experimental metrics for related Nindigo derivatives (Supporting Information). The agreement between theory and experiment for **2c** is also very good (Table 3) for this absorption band and, as is the case for indigo, the transition is exclusively HOMO to LUMO in nature. The frontier orbitals of **2c** are very similar to those of indigo (Figure 4); the isolobal replacement of O by NR does not lead to significant changes in the frontier orbital composition. Qualitatively, the HOMO and LUMO energies of **2c** are raised relative to those of indigo, the

overall consequence of which is a very modest change in the lowest energy absorption maximum. This is the only low-energy transition predicted for **2c** (and for all derivatives of **2**), which contrasts the experimental data: in addition to a dominant absorption at 580–590 nm, the spectra of most Nindigo derivatives also include a weaker, broader absorption near 650 nm.¹⁰ Indigo itself only has the lone low-energy band near 600 nm, but at higher concentrations new absorptions appear which are consistent with solution aggregation.^{19,17} We have ruled out the possibility of aggregation-based origins for the additional absorptions near 650 nm in Nindigo derivatives.¹⁰ At this stage the origin of this “rogue” low energy band is unknown. The excellent correlation with experiment for indigo and the dominant visible band in derivatives of **2** suggests that the calculations are not in error, though this cannot be ruled out. Another possible explanation may involve some combination of tautomerism (H⁺ transfer) and isomerization, for which there is some precedent in the “parent” Nindigo (**2**, R = H).²⁰ We are currently exploring this facet of Nindigo’s spectroscopy further.

Comparisons between the computations on **2c** and the less sterically hindered **2a** are noteworthy. Similarly to **2c**, the low energy transition for **2a** is predicted to be HOMO→LUMO in nature, but the predicted λ_{max} for **2a** (624 nm) is nearly 50 nm longer than that of **2c** (575 nm), and the agreement of the former value with experiment (597 nm) is poorer (error of 1450 cm⁻¹ for **3a** vs 326 cm⁻¹ for **3c**). Inspection of the HOMO and LUMO of **2a** reveals a small but non-negligible contribution from the N-phenyl π manifold (Figure 5) which is

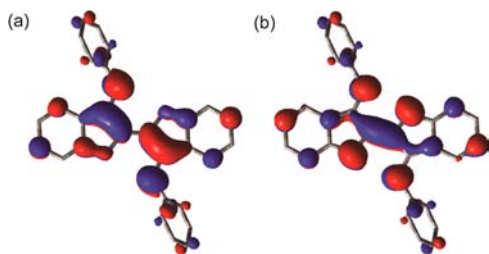


Figure 5. (a) HOMO and (b) LUMO of **2a**.

completely absent in **2c** (Figure 4). This additional delocalization in **2a** (which does not appear to be corroborated by experiment) is a consequence of the torsion angle between the N-aryl substituent plane and that of the Nindigo core being substantially different: for **2c** the calculated torsion angle is 88° while for **2a** the corresponding value is 57°. These trends are qualitatively reproduced in the crystal structures; Nindigo derivatives with bulkier derivatives (**2c**, **2d**) have torsion angles above 80° while those lacking ortho substituents (**2b**,¹⁰ and a *p*-fluorophenyl analogue of **2a**²¹) are smaller but variable (30–70°). However, it appears that the calculations overestimate the degree of involvement of the N-aryl groups in predicting the solution spectral properties of **2a**.

We previously reported calculations on **5a** and **7a** which appeared to provide good agreement with experiment in terms of the lowest energy absorption wavelength, despite the fact that some of the calculated bond metrics for **7a** did not agree particularly well with experiment: experimentally the B–N(indole) and B–N(imine) bonds are 1.536 ± 0.005 Å and 1.561 ± 0.005 Å respectively (average of structures of six different derivatives).¹² The calculated B–N(indole) and B–N(imine) bonds for **7a** are 1.56 and 1.59 Å respectively, and

calculations on the Dmp derivative **7c** reveal the same structural discrepancy. As was the case for the Nindigo ligands, there are significant differences in the calculated torsion angles involving the N–Ar groups for **7a** and **7c** which correlates with a significant difference in $\lambda_{\text{max}}(\text{calc})$ (639 vs 602 nm respectively). Figure 6 presents the HOMOs and LUMOs for Dmp-

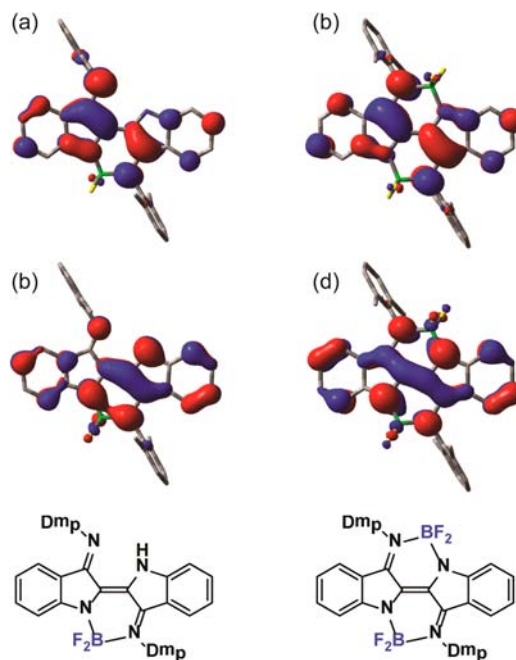


Figure 6. (a) LUMO and (b) HOMO of **7c**; (c) LUMO and (d) HOMO of **5c**.

substituted mono- and bis- BF₂ complexes **7c** and **5c** respectively; the low energy transitions are again predicted to be exclusively HOMO→LUMO in origin. The somewhat larger difference between λ_{calc} and λ_{exp} in **7c** (44 nm) may be related to the structural discrepancies associated with the B–N bonds noted above. In the case of **7a**, these errors are fortuitously countered by the errors stemming from calculated contributions of the N-phenyl substituents (see above). The net result is that the apparent agreement between λ_{calc} and λ_{exp} in **7c** appears to be the result of two different error sources which nearly cancel one another. These qualitative features are also evident in the computational aspects of the bis-BF₂ Nindigo complexes **7a** and **7c**, that is, a relatively large (~30 nm) difference in the calculated λ_{max} values between the two derivatives which is not borne out experimentally, and the apparent relatively close agreement of λ_{calc} and λ_{exp} for **7a** arising from two error sources working in opposite directions.

Replacement of one or both of the BF₂ moieties of **5** by Pd(hfac) groups (i.e., **6** and **3** respectively) attenuates the computational distinctions between the less bulky (phenyl, Ph) and more bulky (2,6-dimethylphenyl, Dmp) imine substituents. The decrease in substituent effect in **6** and **3** can be attributed to the higher twist angles of the N–Ar groups adjacent to palladium, which arises from the larger steric profile of the Pd(hfac) unit compared to BF₂. The differences in $\lambda_{\text{max}}(\text{calc})$ between R = Ph and R = Dmp are 15 nm for **6a/6c** and 13 nm for **3a/3c**; both values are smaller than the corresponding ones for **5a/5c** (27 nm), **7a/7c** (37 nm) or the ligand itself **2a/2c** (49 nm). The agreement between experiment and theory for the Pd-containing complexes is very good; as can be seen in

Table 3, the difference in transition energies for the various Pd-containing complexes fall in the range of 200–400 cm^{-1} —comparable to the discrepancies for the (bulky substituted) Nindigo ligands and indigo itself. Unlike the ligands and boron-containing species, the lowest energy calculated transitions for Pd-containing complexes are a mix of HOMO–LUMO and either HOMO→LUMO+2 (for **6**) or HOMO→LUMO+4 (for **3**). The HOMOs and LUMOs for both complexes (Figure 7)

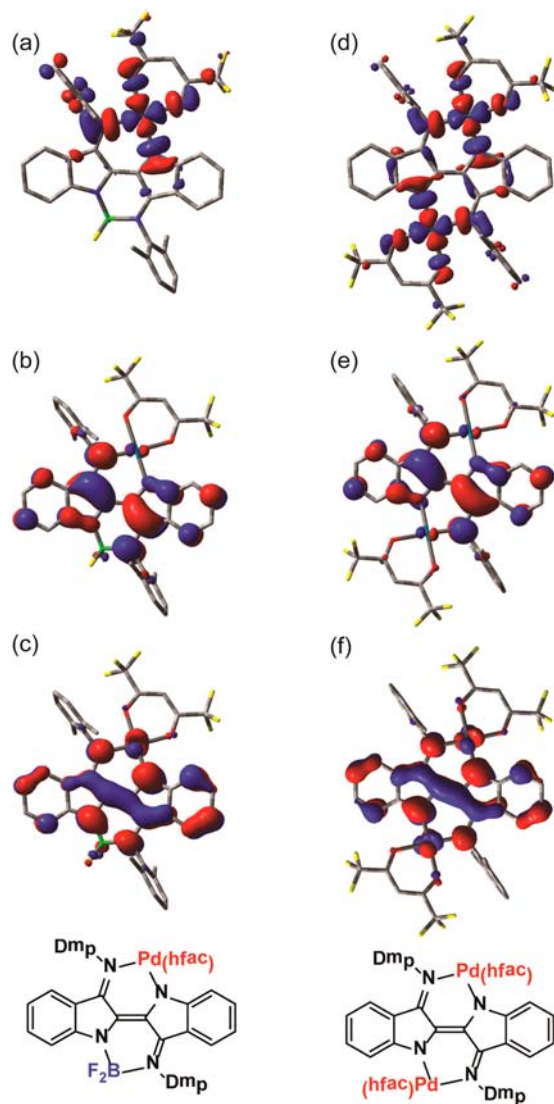


Figure 7. (a) LUMO + 2, (b) LUMO, and (c) HOMO of **6c**; (d) LUMO+4, (e) LUMO, and (f) HOMO of **3c**.

are broadly analogous to the ligand-centered π manifolds for other related compounds, but now with a small contribution to these orbitals from the Pd ion. The higher lying orbitals implicated in the low energy transitions are σ^* in nature based on the Pd $d(x^2-y^2)$ orbital (in the case of bis-Pd complex **3c** the orbital can be described as a linear combination of σ^* orbitals at each Pd center).

CONCLUSIONS

Nindigo presents as a very rare example of a potentially tunable bridging ligand, whereby the R groups offer the possibility of steric/electronic control. The only other examples of bridging ligands with similar potential are Bielawski's bis(carbene)²² and

Cowley's tetrakis(imino)pyracene.²³ However, in the small number of complexes of Nindigo (structure types **2–6**) reported thus far,^{8–10,12} the physicochemical (color, redox) properties of the complexes appear to be dominated by the ligand. Herein we've conducted a systematic experimental and computational investigation of the modulation of Nindigo's properties as a function of what it is coordinated to, facilitated by the synthesis of the first heterobimetallic complexes of this ligand system. The nominally ligand-centered origin of the redox-activity and low-energy absorption is sensitive to the nature of the fragments to which it coordinates, thereby offering the possibility of color and redox tuning via metal coordination. This idea can be considered as an inversion of the usual concept of ligand design, where *ligand* manipulation facilitates control of the *metal*-based properties. In this context it is interesting to speculate about Nindigo-based heterobimetallics in which both metals (unlike tetrahedral boron) can actively contribute to chromophore properties in a “push–pull” manner.

EXPERIMENTAL SECTION

General Considerations. All reactions and manipulations were carried out under an argon atmosphere using standard Schlenk or glovebox techniques unless stated otherwise. All reagents were purchased from Aldrich and used as received. Nindigo-BF₂ complexes **6** and Pd(hfac)₂²⁴ were prepared according to literature procedures. Dichloromethane was stored over CaH₂ and distilled prior to use. NMR spectra were recorded at room temperature on either 300 or 500 MHz instruments. Electronic spectra were recorded on a Perkin-Elmer Lambda 1050 instrument in CD₂Cl₂. Cyclic voltammetry experiments were performed with a Bioanalytical Systems CV50 voltammetric analyzer. Typical electrochemical cells consisted of three-electrode setup including a glassy carbon working electrode, platinum counter electrode, and silver quasi-reference electrode. Dichloromethane solutions of the analyte (1 mM) and electrolyte (0.1 M Bu₄N⁺BF₄⁻) were referenced against an internal standard (1 mM Fc). X-ray solution data are summarized in Table 4.

Computational Studies. Density functional theory (DFT) calculations employed the Gaussian 09 (Revision C.01) program²⁵ and the B3LYP²⁶ or the CAM-B3LYP²⁷ exchange-correlation functionals. Optimized geometries were calculated using the 6-31G* basis set on all light element, and the LANL2DZ set²⁸ was employed for palladium. Frequency calculations (same level of theory) confirmed that the optimized structures were potential energy surface minima. Single point calculations were performed using the TZVP basis set²⁹ on all light atoms and LANL2DZ for Pd. The 30 (or in selected cases, 50) lowest energy electronic transitions were calculated using time-dependent DFT³⁰ (TZVP and LANL2DZ as above) and the polarized continuum model (PCM) was employed to model solvation (solvent = CH₂Cl₂, dielectric $\epsilon = 8.94$).³¹

μ -(Indigodiphenylimine)(hexafluoroacetylacetonatepalladium)-(difluoroboron) **6a**. Compound **7a** (170 mg, 0.370 mmol) was dissolved in 15 mL of DCM. To this solution was added dropwise a solution of Pd(hfac)₂ (1equiv, 193 mg) in 35 mL of DCM. The solution was left to stir overnight. The crude reaction mixture was then extracted three times with water and once with brine before the organic layer was dried to give a dark powder (270 mg, 94.0%). X-ray quality crystals were grown by slow evaporation of a saturated tetrahydrofuran (THF) solution. ¹H NMR (300 MHz, CDCl₃, 293 K): δ 5.8 (1H, d, $J = 8.1$ Hz), 6.1 (1H, d, $J = 7.9$ Hz), 6.2 (1H, s), 6.5 (1H, t, $J = 7.6$ Hz), 6.5 (1H, t, $J = 7.9$ Hz), 7.3 (m, 5H), 7.5 (m, 9H). ¹³C NMR (500 MHz, CD₂Cl₂, 293 K): δ = 93.2, 115.7, 116.3 (q, CF₃, $J = 284.1$ Hz), 117.2, (q, CF₃, $J = 285.6$ Hz), 117.3, 119.4, 120.0, 120.2, 121.4, 125.5, 126.9, 127.1, 128.4, 128.5, 129.3, 130.2, 130.3, 132.6, 135.0, 135.6, 141.1, 145.9, 152.7, 157.6, 158.4, 159.0, 174.8 (q, CO, $J = 35.6$ Hz), 175.7 (q, CO, $J = 35.2$ Hz). ¹⁹F NMR (300 MHz, CD₂Cl₂, 293 K): δ = -130.5 (1:1:1:1 q, $J = 29.2$ Hz), -74.8, -73.4. ¹¹B NMR

Table 4. X-ray Structure Solution Data

	6a-0.5 THF	6c-0.5 MeCN	6d-CH ₂ Cl ₂
empirical formula	C ₃₅ H ₂₃ BF ₈ N ₄ O _{2.5} Pd	C ₃₈ H _{28.5} BF ₈ N _{4.5} O ₂ Pd	C ₄₆ H ₄₃ BCl ₂ F ₈ N ₄ O ₂ Pd
formula wt.	808.78	849.36	1025.97
T (K)	173	173	173
wavelength (Å)	0.71073	0.71073	0.71073
crystal system	triclinic	monoclinic	triclinic
space group	P $\bar{1}$ (No. 2)	Pc (No. 7)	P $\bar{1}$ (No. 2)
a (Å)	11.3192 (8)	15.1584 (6)	9.4672 (3)
b (Å)	12.4363 (9)	11.8641 (4)	14.2029 (5)
c (Å)	13.4483 (10)	19.9033 (7)	17.3360 (6)
α (deg)	83.4965 (8)	90	78.0317 (4)
β (deg)	68.0361 (8)	105.0514 (4)	88.9814 (4)
γ (deg)	64.4777 (8)	90	76.9012 (4)
V (Å ³)	1581.8 (2)	3456.6 (2)	2219.98 (13)
Z	2	4	2
μ (mm ⁻¹)	0.677	0.623	0.616
ρ_{calc} (g/cm ³)	1.698	1.632	1.535
data collected	14113	30380	19880
unique data	7276	15822	10238
parameters	543	992	577
G.o.F.	1.049	1.016	1.055
R ₁	0.0356	0.0281	0.0433
wR ₂ (all data)	0.1012	0.0704	0.1293
CCDC#	908423	908424	908425

(500 MHz, CD₂Cl₂, 293 K): δ = 1.50 (t, J = 29.2 Hz). UV/vis/NIR (CD₂Cl₂), $\lambda_{\text{max}}/\text{nm}$ (ϵ , M⁻¹ cm⁻¹): 307 (42,900), 367 (12,200), 385 (11,600), 409 (8,620), 822 (19,200). HRMS, m/z : calcd for (M)⁺ C₃₃H₁₉N₄BF₈O₂Pd 722.0508; found 772.0512.

μ -Indigobis(*p*-methylphenylamine)(hexafluoroacetylacetonate-palladium)(difluoroboron) **6b**. Compound **7b** (38 mg, 0.0788 mmol) was dissolved in 15 mL of DCM. To this solution was added dropwise a solution of Pd(hfac)₂ (1 equiv, 41 mg) in 35 mL of DCM. The solution was left to stir overnight. It was then extracted 3 times with water before the organic layer was pumped dry. The dark solid was dissolved in a minimal amount of DCM and run through a basic alumina column and dried (48 mg, 76%). X-ray quality crystals were grown by slow diffusion of acetonitrile into a saturated DCM solution. ¹H NMR (300 MHz, CD₂Cl₂, 293 K): δ = 2.4 (3H, s), 2.5 (3H, s), 6.0 (1H, d, J = 8.2 Hz), 6.2 (1H, d, J = 7.5 Hz), 6.3 (1H, s), 6.5 (1H, dodod, J = 7.2 Hz, J = 7.2 Hz, J = 1.8 Hz), 6.6 (1H, dodod, J = 7.2 Hz, J = 6.0 Hz, J = 1.8 Hz), 7.1 (1H, d, 8.3 Hz), 7.2 (1H, dodod, J = 8.7 Hz, J = 6.6, J = 1.4 Hz), 7.3 (8H, m), 7.5 (1H, d, J = 8.7 Hz). ¹³C¹H NMR (500 MHz, CD₂Cl₂, 293 K): δ = 21.6 (CH₃), 93.2 (CH, hfac), 115.2 (CF₃), 115.6 (CH), 117.2 (CH), 119.5 (C^q), 120.1 (CH), 121.3 (CH), 125.1 (CH), 126.5 (CH), 127.0 (CH), 127.2 (CH), 128.5 (C^q), 130.7 (CH), 130.8 (CH), 132.5 (C^q), 134.8 (CH), 135.5 (CH), 138.5 (C^q), 138.8 (C^q), 139.6 (C^q), 143.3 (C^q), 152.7 (C^q), 158.5 (C^q), 158.9 (C^q), 157.5 (C^q), 174.8 (q, CO, J = 34.6 Hz), 175.7 (q, CO, J = 35.0 Hz). ¹⁹F¹H NMR (300 MHz, CD₂Cl₂, 293 K): δ = -130.8 (1:1:1:1 q, J = 29.4 Hz), -75.2, -73.8. ¹¹B¹H NMR (500 MHz, CD₂Cl₂, 293 K): δ = 1.5 (t, J = 29.4 Hz). UV/vis/NIR (CH₂Cl₂), $\lambda_{\text{max}}/\text{nm}$ (ϵ , M⁻¹ cm⁻¹): 307 (45,700), 366 (11,900), 385 (11,600), 409 (8,760), 820 (19,900). HRMS, m/z : calcd for (M)⁺ C₃₅H₂₃N₄BF₈O₂Pd 800.0821; found 800.0827.

μ -Indigobis(2,6-dimethylphenylamine)(hexafluoroacetylacetonate-palladium)(difluoroboron) **6c**. Compound **7c** (44 mg, 0.085 mmol) was dissolved in DCM (15 mL). To this solution was added dropwise a solution of Pd(hfac)₂ (1 equiv, 44 mg) in DCM (35 mL). The solution was left to stir overnight. It was then extracted 3 times with water before the organic layer was pumped dry. The dark solid was dissolved in a minimal amount of DCM and run through a basic alumina column and dried (54 mg, 76.7%). ¹H NMR (300 MHz, CD₂Cl₂, 293 K): δ = 2.2 (s, 6H), 2.3 (s, 6H), 5.8 (d, 1H, J = 8.1 Hz), 5.9 (1H, d, J = 8.2 Hz), 6.3 (1H, s), 6.5 (1H, t, J = 7.7 Hz), 6.1 (1H,

m), 7.3 (9H, m), 7.6 (1H, d, J = 8.7 Hz). ¹³C¹H NMR (500 MHz, CD₂Cl₂, 293 K): δ = 174.9 (q, CO, J = 34.7 Hz), 176.0 (q, CO, J = 36.3 Hz). ¹⁹F¹H NMR (300 MHz, CD₂Cl₂, 293 K): δ = -73.7 (s), -75.3 (s), -130.7 (q, J = 28.9 Hz). ¹¹B¹H NMR (500 MHz, CD₂Cl₂, 293 K): δ = 1.7 (t, J = 29.9 Hz). UV/vis/NIR (CH₂Cl₂), $\lambda_{\text{max}}/\text{nm}$ (ϵ , M⁻¹ cm⁻¹): 306 (39,900), 366 (8,970), 385 (8,270), 409 (5,620), 819 (17,500). HRMS, m/z : calcd for (M)⁺ C₃₇H₂₇N₄BF₈O₂Pd: 828.1134; found 828.1140

μ -Indigobis(2,3-diisopropylphenylamine)(hexafluoroacetylacetonate-palladium)(difluoroboron) **6d**. Compound **7d** (82 mg, 0.13 mmol) was dissolved in DCM (15 mL). To this solution was added dropwise a solution of Pd(hfac)₂ (1 equiv, 68 mg) in DCM (35 mL). The resultant solution was left to stir overnight. It was then extracted 3 times with water before the organic layer was pumped dry. The dark solid was dissolved in a minimal amount of DCM and run through a basic alumina column and dried (88 mg, 72.2%). ¹H NMR (300 MHz, CD₂Cl₂, 293 K): δ = 0.9 (d, 12H, J = 6.8 Hz), 1.0 (d, 12H, J = 6.8 Hz), 1.3 (d, 12H, J = 2.2 Hz), 1.3 (d, 12H, J = 2.0 Hz), 3.1 (septet, 2H, J = 6.7 Hz), 3.4 (septet, 2H, J = 6.8 Hz), 5.7 (1H, d, J = 8.3 Hz), 5.9 (1H, d, J = 8.3 Hz), 6.3 (s, 1H), 6.5 (t, 1H, J = 7.3 Hz), 6.6 (dodod, 1H, J = 8.3 Hz, J = 6.4 Hz, J = 1.8 Hz), 7.2 (dodod, 1H, J = 8.7 Hz, J = 7.2 Hz, J = 1.5 Hz), 7.4 (m, 6H), 7.6 (m, 2H), 7.7, d, 1H, J = 8.7 Hz). ¹³C¹H NMR (500 MHz, CD₂Cl₂, 293 K): δ = 23.6, 24.1, 24.1, 24.8, 28.9, 93.1, 115.7, 116.8, 119.7, 119.8, 121.1, 125.0, 125.2, 126.6, 127.0, 128.9, 129.4, 134.7, 135.5, 135.6, 140.7, 142.3, 145.4, 152.2, 156.5, 156.6, 158.9, 159.0. ¹⁹F¹H NMR (300 MHz, CD₂Cl₂, 293 K): δ = -129.0 (1:1:1:1 q, J = 29.3 Hz), -75.0, -73.5. ¹¹B¹H NMR (500 MHz, CD₂Cl₂, 293 K): δ = 1.5 (t, J = 29.3 Hz). UV/vis/NIR (CH₂Cl₂), $\lambda_{\text{max}}/\text{nm}$ (ϵ , M⁻¹ cm⁻¹): 307 (41,600), 366 (9,230), 385 (8,440), 409 (5,550), 820 (20,700). HRMS, m/z : calcd for (M)⁺ C₄₅H₄₃N₄BF₈O₂Pd 940.2386; found 940.2386

■ ASSOCIATED CONTENT

Supporting Information

Crystallographic data files (CIF format) and additional experimental and computational data. This material is available free of charge via the Internet at <http://pubs.acs.org>.

AUTHOR INFORMATION

Corresponding Author

*E-mail: rhichs@uvic.ca.

Notes

The authors declare no competing financial interest.

ACKNOWLEDGMENTS

We thank the University of Victoria and the Natural Sciences and Engineering Research Council of Canada for support. Computational work was made possible by the facilities of the WestGrid Computing Network.

REFERENCES

- (1) (a) Ward, M. D.; McCleverty, J. A. *J. Chem. Soc., Dalton Trans.* **2002**, 275–288. (b) Kaim, W. *Inorg. Chem.* **2011**, *50*, 9752–9765.
- (2) Lyaskovskyy, V.; de Bruin, B. *ACS Catal.* **2012**, *2*, 270–279.
- (3) (a) Chirik, P. J. *Inorg. Chem.* **2011**, *50*, 9737–9740. (b) de Bruin, B. *Eur. J. Inorg. Chem.* **2012**, 340–342.
- (4) (a) Wada, T.; Tsuge, K.; Tanaka, K. *Angew. Chem., Int. Ed.* **2000**, *39*, 1479–1482. (b) Stanciu, C.; Jones, M. E.; Fanwick, P. E.; Abu-Omar, M. M. *J. Am. Chem. Soc.* **2007**, *129*, 12400–12401. (c) Blackmore, K. J.; Lal, N.; Ziller, J. W.; Heyduk, A. F. *J. Am. Chem. Soc.* **2008**, *130*, 2728–2729. (d) Ringenberg, M. R.; Kokatam, S. L.; Heiden, Z. M.; Rauchfuss, T. B. *J. Am. Chem. Soc.* **2008**, *130*, 788–9. (e) Zarkesh, R. A.; Ziller, J. W.; Heyduk, A. F. *Angew. Chem., Int. Ed.* **2008**, *47*, 4715–4718. (f) Lippert, C. A.; Arnstein, S. A.; Sherrill, C. D.; Soper, J. D. *J. Am. Chem. Soc.* **2010**, *132*, 3879–3892. (g) Smith, A. L.; Hardcastle, K. I.; Soper, J. D. *J. Am. Chem. Soc.* **2010**, *132*, 14358–14360. (h) Kraft, S. J.; Williams, U. J.; Daly, S. R.; Schelter, E. J.; Kozimor, S. A.; Boland, K. S.; Kikkawa, J. M.; Forrest, W. P.; Christensen, C. N.; Schwarz, D. E.; Fanwick, P. E.; Clark, D. L.; Conradson, S. D.; Bart, S. C. *Inorg. Chem.* **2011**, *50*, 9838–9848.
- (5) (a) Bouwkamp, M. W.; Bowman, A. C.; Lobkovsky, E.; Chirik, P. J. *J. Am. Chem. Soc.* **2006**, *128*, 13340–13341. (b) Knijnenburg, Q.; Gambarotta, S.; Budzelaar, P. H. M. *Dalton Trans.* **2006**, 5442–5448.
- (6) Dzik, W. I.; Zhang, X. P.; de Bruin, B. *Inorg. Chem.* **2011**, *50*, 9896–9903.
- (7) (a) Donati, N.; Konigsmann, M.; Stein, D.; Udino, L.; Grutzmacher, H. C. R. *Chim.* **2007**, *10*, 721–730. (b) Hicks, R. G. *Angew. Chem., Int. Ed.* **2008**, *47*, 7393–7395. (c) Mankad, N. P.; Antholine, W. E.; Szilagy, R. K.; Peters, J. C. *J. Am. Chem. Soc.* **2009**, *131*, 3878–3880. (d) Wiese, S.; Badiei, Y. M.; Gephart, R. T.; Mossin, S.; Varonka, M. S.; Melzer, M. M.; Meyer, K.; Cundari, T. R.; Warren, T. H. *Angew. Chem., Int. Ed.* **2010**, *49*, 8850–8855. (e) King, E. R.; Hennessy, E. T.; Betley, T. A. *J. Am. Chem. Soc.* **2011**, *133*, 4917–4923.
- (8) Schauer, P. A.; Low, P. J. *Eur. J. Inorg. Chem.* **2012**, 390–411.
- (9) Oakley, S. R.; Nawn, G.; Waldie, K. M.; MacInnis, T. D.; Patrick, B. O.; Hicks, R. G. *Chem. Commun.* **2010**, 46, 6753–6755.
- (10) Nawn, G.; Waldie, K. M.; Oakley, S. R.; Peters, B. D.; Mandel, D.; Patrick, B. O.; McDonad, R.; Hicks, R. G. *Inorg. Chem.* **2011**, *50*, 9826–9837.
- (11) Fortier, S.; González-del Moral, O.; Chen, C. H.; Pink, M.; Le Roy, J. J.; Murugesu, M.; Mindiola, D. J.; Caulton, K. G. *Chem. Commun.* **2012**, 48, 11082–11084.
- (12) Nawn, G.; Oakley, S. R.; Majewski, M. B.; McDonad, R.; Patrick, B. O.; Hicks, R. G. *Chem. Sci.* **2013**, *4*, 612–621.
- (13) (a) Evans, D. H.; Hu, K. *J. Chem. Soc., Faraday Trans.* **1996**, *92*, 3983–3990. (b) Evans, D. H. *Chem. Rev.* **2008**, *108*, 2113–2144.
- (14) Jacquemin, D.; Perpète, E. A.; Scuseria, G. E.; Ciofini, I.; Adamo, C. *J. Chem. Theory Comput.* **2008**, *4*, 123–135.
- (15) Jacquemin, D.; Perpète, E. A.; Ciofini, I.; Adamo, C. *Acc. Chem. Res.* **2009**, *42*, 326–334.
- (16) (a) Guillaumont, D.; Nakamura, S. *Dyes Pigments* **2000**, *46*, 85–92. (b) Jacquemin, D.; Preat, J.; Wathelet, V.; Fontaine, M.; Perpète, E. A. *J. Am. Chem. Soc.* **2006**, *128*, 2072–2083. (c) Jacquemin, D.; Preat, J.; Wathelet, V.; Perpète, E. A. *J. Chem. Phys.* **2006**, *124*, 074104. (d) Fabian, J. *Dyes Pigments* **2010**, *84*, 36–53.
- (17) Amat, A.; Rosi, F.; Miliani, C.; Sgamellotti, A.; Fantacci, S. *J. Mol. Struct.* **2011**, *993*, 43–51.
- (18) (a) Wille, E.; Luttke, W. *Angew. Chem., Int. Ed. Engl.* **1971**, *10*, 803–804. (b) Wille, E.; Luttke, W. *Liebigs Ann. Chem.* **1980**, 2039–2054.
- (19) Miliani, C.; Romani, A.; Favaro, G. *Spectrochim. Acta* **1998**, *A54*, 581–588.
- (20) (a) Thoburn, J. D.; Luttke, W.; Benedict, C.; Limbach, H. H. *J. Am. Chem. Soc.* **1996**, *118*, 12459–12460. (b) Sieghold, H.; Luttke, W. *Angew. Chem., Int. Ed. Engl.* **1975**, *14*, 52–52.
- (21) Boeyens, J. C. A.; Cook, L. M.; Ding, Y. X.; Fernandes, M. A.; Reid, D. H. *Org. Biomol. Chem.* **2003**, *1*, 2168–2172.
- (22) Tennyson, A. G.; Ono, R. J.; Hudnall, T. W.; Khramov, D. M.; Er, J. A. V.; Kamplain, J. W.; Lynch, V. M.; Sessler, J. L.; Bielawski, C. W. *Chem.—Eur. J.* **2010**, *16*, 304–315.
- (23) (a) Vasudevan, K. V.; Findlater, M.; Cowley, A. H. *Chem. Commun.* **2008**, 1918–1919. (b) Vasudevan, K. V.; Vargas-Baca, I.; Cowley, A. H. *Angew. Chem., Int. Ed.* **2009**, *48*, 8369–8371. (c) Vasudevan, K. V.; Cowley, A. H. *New J. Chem.* **2011**, *35*, 2043–2046. (d) Vasudevan, K. V.; Findlater, M.; Vargas-Baca, I.; Cowley, A. H. *J. Am. Chem. Soc.* **2012**, *134*, 176–178.
- (24) Zharkova, G. I.; Stabnikov, P. A.; Sysoev, S. A.; Igumenov, I. K. *J. Struct. Chem.* **2005**, *46*, 320–327.
- (25) Frisch, M. J.; Trucks, G. W.; Schlegel, H. B.; et al. *Gaussian 09*, Revision B.1; Gaussian, Inc.: Wallingford, CT, 2009.
- (26) (a) Becke, A. D. *J. Chem. Phys.* **1993**, *98*, 5648–5652. (b) Stephens, P. J.; Devlin, F. J.; Chabalowski, C. F.; Frisch, M. J. *J. Phys. Chem.* **1994**, *98*, 11623–11627.
- (27) (a) Tawada, Y.; Tsuneda, T.; Yanagisawa, S.; Yanai, T.; Hirao, K. *J. Chem. Phys.* **2004**, *120*, 8425–8433. (b) Yanai, T.; Tew, D. P.; Handy, N. C. *Chem. Phys. Lett.* **2004**, *393*, 51–57.
- (28) (a) Hay, P. J.; Wadt, W. R. *J. Chem. Phys.* **1985**, *82*, 270. (b) Hay, P. J.; Wadt, W. R. *J. Chem. Phys.* **1985**, *82*, 299.
- (29) Schafer, A.; Horn, H.; Ahlrichs, R. *J. Chem. Phys.* **1992**, *97*, 2571–2577.
- (30) (a) Casida, M. E. In *Recent Advances in Density Functional Methods*; Chong, D. P., Ed.; World Scientific: Singapore, 1995; p 155; (b) Stratmann, R. E.; Scuseria, G. E.; Frisch, M. J. *J. Chem. Phys.* **1998**, *109*, 8218–8224.
- (31) (a) Barone, V.; Cossi, M.; Tomasi, J. *J. Chem. Phys.* **1997**, *107*, 3210–3221. (b) Barone, V.; Cossi, M.; Tomasi, J. *J. Comput. Chem.* **1998**, *19*, 404–417. (c) Miertus, S.; Scrocco, E.; Tomasi, J. *J. Chem. Phys.* **1981**, *55*, 117–129.